The Optimally Performing Fischer–Tropsch Catalyst

Ivo A. W. Filot, Rutger A. van Santen, and Emiel J. M. Hensen*

Abstract: *Microkinetics simulations are presented based on DFT-determined elementary reaction steps of the Fischer–Tropsch (FT) reaction. The formation of long-chain hydrocarbons occurs on stepped Ru surfaces with CH as the inserting monomer, whereas planar Ru only produces methane because of slow CO activation. By varying the metal–carbon and metal–oxygen interaction energy, three reactivity regimes are identified with rates being controlled by CO dissociation, chain-growth termination, or water removal. Predicted surface coverages are dominated by CO, C, or O, respectively. Optimum FT performance occurs at the interphase of the regimes of limited CO dissociation and chain-growth termination. Current FT catalysts are suboptimal, as they are limited by CO activation and/or O removal.*

The Fischer–Tropsch (FT) process converts synthesis gas into longer hydrocarbons and has become the subject of an intensive research effort driven by the increasing value of liquid energy carriers compared to the ample supply of natural gas.[1] The heterogeneous Fischer–Tropsch reaction is mechanistically complex. Unravelling the relation between the chemical reactions at the surface and the composition of the adsorbed layer poses a great challenge. The mechanism essentially combines a polymerization-type surface reaction, which produces mainly linear hydrocarbons, with the in situ generation of monomers containing a single C atom. Many uncertainties exist on the nature of the reaction intermediates and hence also on the relative rates of the elementary reaction steps.

Advances in computational catalysis enable detailed studies of surface reactions at the molecular level, thus generating important new and comprehensive information about the relation between the relative stability of surface intermediates and their rate of formation and conversion as a function of catalyst composition and structure.

With respect to the important question of selectivity of the FT reaction, according to one school of thought, small particles are not reactive, as strongly adsorbed CO inhibits chain growth;[2,3] according to others, step-edge sites are required that are not stable on small particles.[4–6] This explains the observation that selectivity toward the produc-

tion of methane strongly increases and the rate of CO consumption decreases for smaller transition-metal nano-particles.[5,7] Microkinetics simulations based on computed molecular reactivity data provide a unique opportunity to resolve such debates. Rate-controlling steps can be deduced,[8] and hence one can identify the nature of particular relevant surface intermediates at specific reaction conditions.

The microkinetics simulation presented herein makes use of DFT quantum-chemical data of the elementary reaction rates of the many reaction intermediates proposed in FT catalysis.[1,9–13] Few of such complete studies exist that not only consider the formation of methane,[14] but also include the formation of longer hydrocarbon chains. Earlier microkinetics studies are available that used approximate molecular reactivity data.[6,15–17] Data for the Ru$(11\bar{2}1)$ surface will be compared with predictions for the Ru(0001) surface. A summary of these data and details of the microkinetic implementation are given in the Supporting Information. The DFT results have been discussed in another paper.[18]

The stepped Ru$(11\bar{2}1)$ surface was chosen because its reactive centers have a low barrier for CO activation and bind reaction intermediates strongly.[19,20] Because the metal–carbon interaction energy is relatively strong, we expected it to show a low rate of formation of methane compared to the production of longer hydrocarbons.[21] We compared it with the dense Ru(0001) surface, because this surface has a high barrier for CO activation and can therefore be expected to have a high selectivity for the production of methane. Amongst others, these expectations are based on our previous work with approximate and sometimes estimated values of reaction intermediate data.[6,15,16]

The microkinetics simulation data on the Ru$(11\bar{2}1)$ surface showed that under the conditions of the optimum C_{20+} yield, the reaction rate is controlled by the rate of water formation. This causes the CO consumption rate to be slow with the surface predominantly covered by O atoms. We have extended these results to reactivity regimes of other catalyst materials by varying the computed reactivity parameters of reaction intermediates using scaling rules,[22] relating the stability of surface species with adsorption energies of atomic C and O as reactivity performance parameters. By using Brønsted–Evans–Polanyi (BEP) relations[23,24] in addition to the aforementioned scaling relations, we have constructed a two-dimensional volcano plot[12,25] of CO consumption rate, selectivity, and other relevant kinetic parameters. Three different reactivity regimes can be identified, that is, previously proposed[15,16] regimes limited by monomer formation and chain-growth termination as well as a regime where oxygen removal is limiting. The maximum of the CO consumption rate is located in between these regimes.

Our model, which takes into account both the carbide and the CO insertion mechanism,[26] is defined in detail in the

[*] I. A. W. Filot, Prof. Dr. R. A. van Santen, Prof. Dr. E. J. M. Hensen
Schuit Institute of Catalysis, Department of Chemical Engineering and Chemistry, Eindhoven University of Technology
PO Box 513, 5600 MB, Eindhoven (The Netherlands)
and
Institute for Complex Molecular Systems
Eindhoven University of Technology
PO Box 513, 5600 MB, Eindhoven (The Netherlands)
E-mail: e.j.m.hensen@tue.nl

Supporting information for this article is available on the WWW under http://dx.doi.org/10.1002/anie.201406521.

Supporting Information. All elementary reactions steps, that is, direct and hydrogen-activated CO dissociation, CH_x hydrogenation, CH_x–CH_y coupling, CH_x–CO coupling, CH_xC–O bond scission, and desorption of hydrocarbon chains as olefins and paraffins are taken into account. To also partially account for the lateral interactions, the CO adsorption energy is taken as a function of the surface coverage.

Microkinetics results for $Ru(11\bar{2}1)$ show the expected temperature dependence of activity and selectivity (Figure 1). A high probability of chain growth (α) occurs at relatively low temperatures, whereas a high reaction temperature drives the reaction toward CH_4. Olefins are the primary reaction products with more than one carbon atom. Predicted C_1 and C_2 selectivities deviate from the Anderson–Schulz–Flory (ASF) distribution in line with experimental results (Figure S1). The lower C_2 selectivity is due to stronger binding and easier chain growth of ethylene compared to higher olefins.[18] The low CH_4 selectivity on this surface is consistent with the lower overall barrier for chain growth compared to the overall barrier for the formation of methane. The formation of CH_4 is only preferred at high temperature.

To elucidate the salient details of the FT reaction for the $Ru(11\bar{2}1)$ surface, the reaction path from CO and H_2 to hydrocarbons and water was analyzed in detail in a calculated reaction-intermediate flow scheme at the level of the elementary reaction steps (Figure 2). This analysis was performed at $T = 500$ K, as we found that at this particular temperature the selectivity toward C_{20+} hydrocarbons was maximum (see Figure S2). In industry, the formation of long-chain hydrocarbons with minimum formation of CH_4 is preferred. Figure 2 indicates the relative participation of intermediates in particular reaction steps. As CO conversion to longer hydrocarbons proceeds exclusively through the insertion of CH_x intermediates, we omitted CO-insertion pathways. The rate of CO insertion is very low because of the high barrier of CO insertion as previously discussed.[18] The analysis of the reaction path shows the importance of CH as the main inserting surface intermediate. The main chain-growth pathway involves the insertion of CH into adsorbed CR (R = H or alkyl) growing chains. The resulting surface intermediate CHCR is then hydrogenated to CHCHR. It turns out to be preferred to first dehydrogenate the α-C atom of this fragment before hydrogenating the β-CH group, so that the reaction sequence is CHCHR* + * → CCHR* + H* and CCHR* + H* → CCH$_2$R* + *. The latter species is represented in Figure 2 by CR. This sequence represents the main chain-growth mechanism. The predominance of chain growth according to the carbide mechanism[26] with CH is in line with predictions of Cheng et al.[13]

The resulting CR species can undergo two hydrogenation reactions of the α-C atom and one dehydrogenation reaction of the β-CH_2R group to produce the adsorbed olefin CH_2CHR^*. This CH_2CHR^* intermediate can either desorb from the surface as the 1-olefin or undergo another dehydrogenation of the α-C atom to form CHCHR*, which is an intermediate in the chain-propagation route. The high probability of chain growth at intermediate temperature stems from the higher rate of dehydrogenation compared to desorption. Oxygen removal through the formation of water predominantly proceeds through proton migration between two hydroxy groups.

To underpin the importance of the stepped surface for facile CO dissociation, we carried out additional calculations for the less reactive dense Ru(0001) surface. We used reported data for the dissociation of CO on this surface.[27,28] Because of the high direct CO dissociation barrier (> 200 kJ mol^{-1})[20,28] the route via formyl (overall barrier 146 kJ mol^{-1})[28] dominates. To model the FT reaction for Ru(0001), for all other elementary reactions we employed kinetic data determined for the $Ru(11\bar{2}1)$ surface. Under conditions that predict good FT performance for $Ru(11\bar{2}1)$, the planar Ru(0001) surface only produces methane. Besides difficult CO dissociation, this is also due to a more facile formation of methane from adsorbed C on Ru(0001) (21 kJ mol^{-1}) compared with $Ru(11\bar{2}1)$ (86 kJ mol^{-1}). The CO consumption rate is much lower than for the stepped surface.

The conditions for optimal catalytic performance were then analyzed by evaluating the consequences of variations in the activation energies of the elementary reaction steps. These can be related to the interaction energies of the transition-metal surface with C and O adatoms using BEP and scaling law principles. The approach to compute the activa-
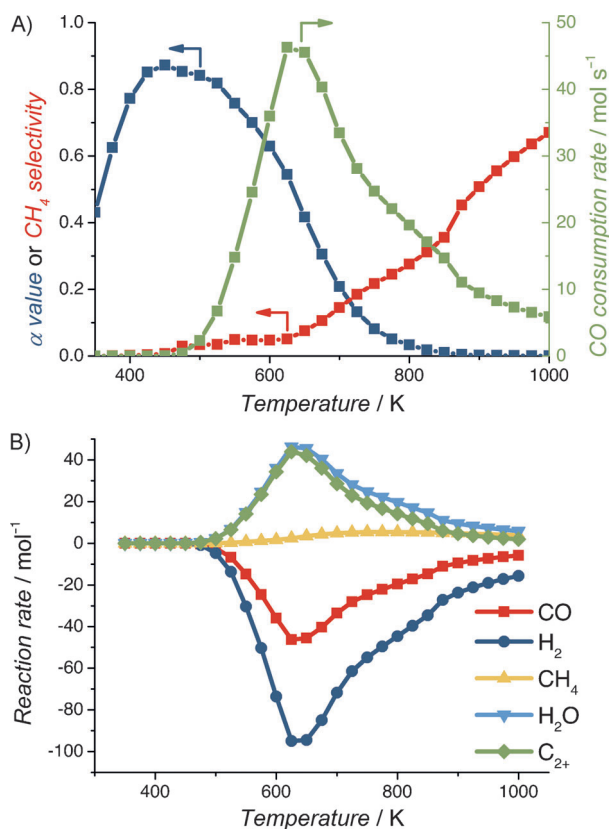

Figure 1. Microkinetics simulations for the $Ru(11\bar{2}1)$ surface ($p = 20$ atm; $H_2/CO = 2$). A) FT CO consumption rate (green), probability of chain growth (blue), and selectivity for the production of methane (red). B) CO (red) and H_2 (dark blue) consumption rates (negative), and CH_4 (yellow), H_2O (light blue), and C_{2+} (green) production rates (positive) as a function of the temperature.
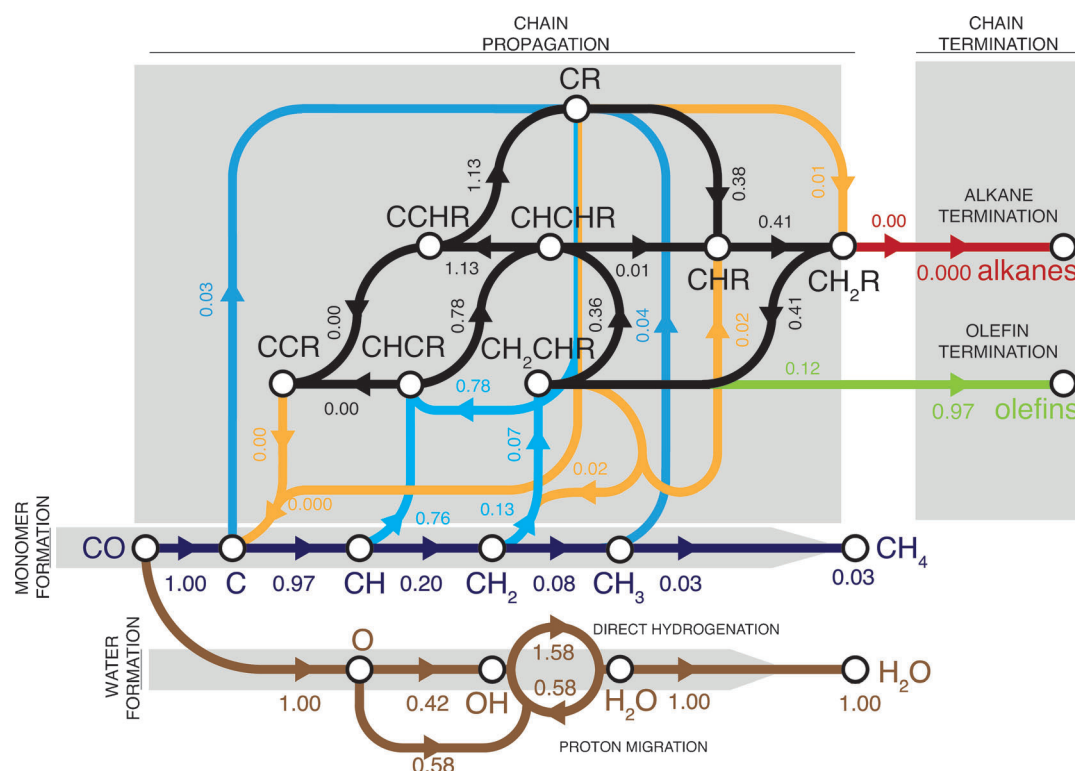
Figure 2. Reaction path analysis for the FT reaction on Ru(11$\bar{2}$1) ($T = 500$ K; $p = 20$ bar; $H_2/CO = 2$). The nodes represent reactants, surface intermediates, and products, the lines between them the elementary reaction steps and the numbers molar rates.

tion energies of the various elementary reaction steps relevant to our microkinetic model is outlined in the Supporting Information. Relevant to the discussion below, we exemplify this by the dependence of the activation barrier for CO dissociation on the strength of the metal−C (ΔE_C) and metal−O (ΔE_O) bond through

$$\Delta\left(\Delta E_a^{CO}\right) = \alpha(\Delta E_C + \Delta E_O). \qquad (1)$$

Figure 3 shows the rate of CO consumption as a function of these interaction energies. Microkinetics simulations were performed at $T = 500$ K, $p = 20$ atm, and $H_2/CO = 2$, because it represents the important case in which wax production is maximized. The CO consumption rate strongly depends on the adatom bond strengths and exhibits a Volcano-type behavior. The predicted rate for the Ru(11$\bar{2}$1) surface is close to the optimum.

Three distinct regimes can be distinguished in Figure 3 on the basis of differences in the rate-controlling step for the overall FT reaction. These regimes will be discussed below. To facilitate the discussion, Figure 3 also contains contour plots for the most important kinetic parameters for the FT reaction as a function of ΔE_C and ΔE_O.

In regime I, the CO consumption rate is controlled by the rate of CO dissociation. The reaction order with respect to CO is positive in this regime. The H_2 reaction order is slightly negative, because increasing H coverage lowers the CO-dissociation rate. The apparent activation energy is close to the activation energy for CO dissociation. Decreasing the reactivity of the metal surface (going to the top right-hand corner of the contour plots) will result in a lower probability

of chain growth (α). A metal with low reactivity, such as Ni, combines a low rate of CO dissociation with facile CH_4 formation.[29] With increasing metal reactivity, the probability of chain growth strongly increases. In regime I, the FT reaction proceeds in the monomer-formation limit, as earlier discussed by us in a lumped kinetics analysis.[16]

In regime II, the rate is limited by the rates of chain growth and chain-growth termination (chain-growth termination limit).[16] Under these conditions, the surface is nearly fully covered with C and CH intermediates. Consistent with this, a degree of rate control (X_{DRC}) analysis (Figure S3) shows that the two reaction steps with the greatest X_{DRC} are hydrogenation of CHCR ($X_{DRC} = 0.7$) and desorption of olefins ($X_{DRC} = 0.3$). The most difficult step is the hydrogenation of CHCR to CHCHR, which is an essential step in the chain-growth mechanism, that is, in the formation of CCH_2R, the intermediate into which the next CH building block can insert. The slightly positive CO reaction order in this regime stems from the inhibiting effect of the C−CR decoupling step ($X_{DRC} = -0.5$), which requires free sites. With increasing CO partial pressure, the fraction of free sites decreases and, accordingly, also the rate of decoupling decreases. This increases the overall CO consumption rate. The H_2 reaction order is strongly positive, because chain growth requires several hydrogenation steps. Typically, the apparent activation energies in this regime are small or can even take negative values. The apparent activation energy is negative, when with increasing temperature vacancies are created as a result of product desorption. The increased vacancy concentration increases the CCR decoupling rate, which lowers the overall CO consumption rate. Figure 3
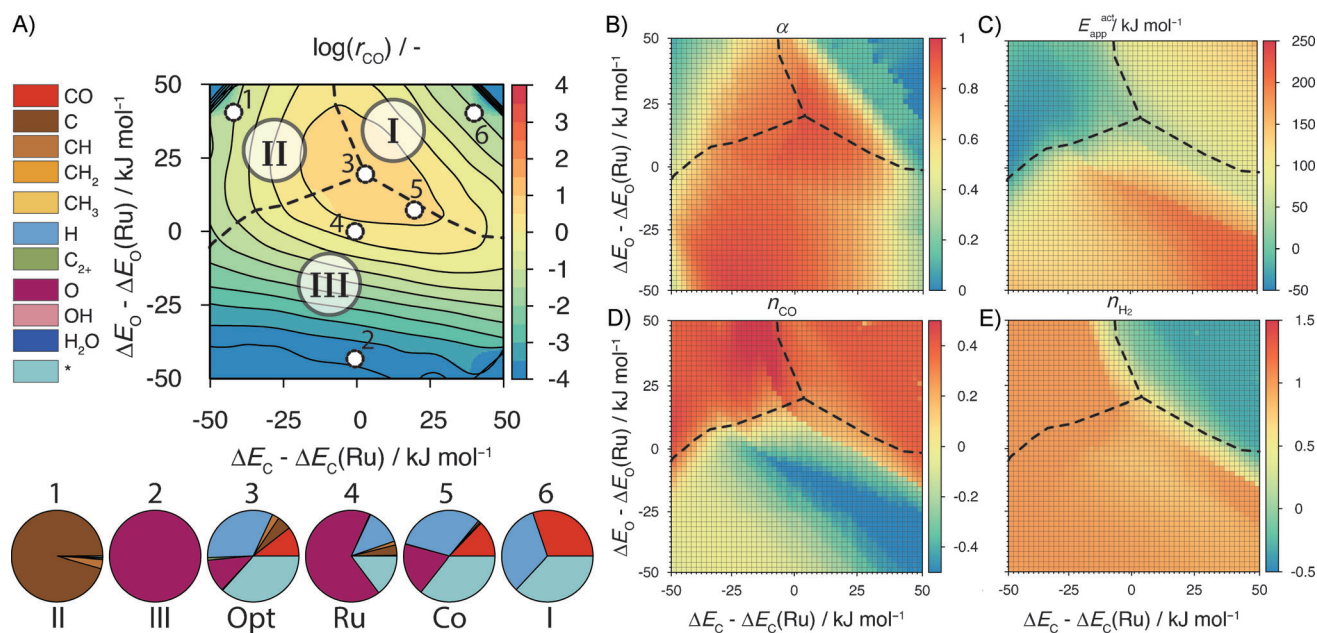
Figure 3. A) CO consumption rate and steady-state surface coverages (the numbers in the graph refer to the numbers above the pie charts) as a function of the metal–carbon and metal–oxygen bond strength ($T = 500$ K; $p = 20$ bar; $H_2/CO = 2$). The activation barriers for all elementary reaction steps were scaled to the metal–carbon and metal–oxygen bond strengths. Three regimes are distinguished based on the nature of the rate-controlling step, that is, CO dissociation (regime I), chain growth and chain-growth termination (regime II), and water formation (regime III). The positions of Ru and Co metals are indicated on the basis of the strengths of their metal–carbon and metal–oxygen bonds. B–E) Simulated kinetic parameters for the FT reaction ($T = 500$ K; $p = 20$ bar; $H_2/CO = 2$) as a function of ΔE_C and ΔE_O relative to the respective values for Ru(112̄1). B) Chain-growth probability, C) apparent activation energy (kJ mol^{-1}), D) reaction order with respect to CO, and E) reaction order with respect to H$_2$.

shows that the probability of chain growth strongly decreases, if the M—C interaction energy becomes very strong, which leads to high activation barriers for the hydrogenation reactions.

While the formation of methane requires only the hydrogenation of the C atom, chain growth requires both hydrogenation of the C atom to CH for monomer insertion as well as subsequent hydrogenation of the growing hydrocarbon chain. Consequently, the formation of methane will become preferred over chain growth at a high metal—C interaction energy.

Regime III is representative for surfaces to which oxygen binds strongly. Then, the removal of water can become the rate-controlling step. Candidate rate-controlling elementary reaction steps are OH hydrogenation to H$_2$O and proton migration between two OH species to form O and H$_2$O. This is consistent with O being the most abundant surface intermediate. High ΔE_O implies that the barrier for CO dissociation is low. Consequently, the CO reaction order is negative. For relatively low ΔE_C the apparent activation energy is very high because the O atom needs to be removed from the surface. When the metal–carbon interaction energy increases, the surface-adsorbed layer will contain an increasing amount of C and CH intermediates as well as growing chains instead of O. This results in an increase of the CO consumption rate and the probability of chain growth, and a decrease of the apparent activation energy. For high ΔE_C, the CO consumption rate and the chain-growth probability decrease again, because C hydrogenation becomes difficult.

The maximum CO consumption rate at $T = 500$ K and $p = 20$ atm is obtained for $\Delta E_C = 2.1$ and $\Delta E_O = 20.2$ kJ mol^{-1}.

Consistent with the Sabatier principle,[23,26] this maximum is the result of the competition of several competing elementary reaction steps. In this case, OH hydrogenation (X$_{DRC} = 0.47$), CO dissociation (X$_{DRC} = 0.19$), CH$_2$ + CHR coupling (X$_{DRC} = 0.12$), C + CR coupling (X$_{DRC} = 0.078$), and CHCHR hydrogenation (X$_{DRC} = 0.045$) determine the maximum of the CO consumption rate. The surface coverages at this optimum are $\theta_{CO} \approx 0.11$, $\theta_O \approx 0.12$, $\theta_H \approx 0.33$, $\theta_C \approx 0.05$, $\theta_{CH} \approx 0.02$, $\theta_{C2+} \approx 0.01$, and $\theta^* \approx 0.37$. The CO and H$_2$ reaction orders are 0.30 and 0.66, respectively, and the apparent activation energy is 37 kJ mol^{-1}. The probability of chain growth is high with 0.92. The reaction order in CO is higher than typically found in experiments, whereas the apparent activation energy is lower.[11,30,31] This indicates that FT synthesis using Ru or Co catalysts is not conducted at the optimum performance potential. Although the simulated catalyst optimum depends on the chosen parameters for the CO adsorption energy, increasing or decreasing the adsorption energy of CO to simulate different CO coverages does not alter this finding (see the Supporting Information).

By comparing the simulated reaction orders and activation energies with experimental data,[11,30–32] we deduce that current FT catalysts operate somewhere between regimes I and II. The FT reaction on Ru metal proceeds in the chain-growth limit with a surface partially poisoned by O adatoms, whereas on Co surfaces the reaction occurs in the monomer-formation limit. In this case, CO dissociation is controlling the rate, consistent with the general assumption in kinetic studies for the Co-catalyzed FT reaction.[10,11,31] Another important aspect of our findings is that in these regimes, the coordinative

unsaturated surface metal atoms in the step-edge site are not poisoned by C adatoms[2] that are formed upon CO dissociation. Our analysis shows that this is because of rapid CH intermediate formation, the key chain-growth monomer. The present work also shows that production of long-chain hydrocarbons is consistent with high CO coverage, as even at relatively high CO coverage a high rate of chain growth can be maintained. Increasing the CO adsorption energy does not change this result, but leads to a shift of the reaction maximum to higher temperatures (see the Supporting Information). Finally, this study identifies sites with a low barrier for CO dissociation as the locus of the FT reaction. This implies that the FT reaction with low selectivity for the production of methane will take place on a relatively small part of the surface of the catalytic nanoparticles.[33] Dense surfaces with low reactivity are the locus of CO hydrogenation to methane.

[1] F. Fischer, H. Tropsch, *Brennst.-Chem.* **1923**, *4*, 276; F. Fischer, H. Tropsch, *Brennst.-Chem.* **1926**, *7*, 79–116.

[2] K. Fei Tan, J. Xu, J. Chang, A. Borgna, M. Saeys, *J. Catal.* **2010**, *274*, 121–129; D. J. Moodley, J. van de Loosdrecht, A. M. Saib, M. J. Overett, A. K. Datye, J. W. Niemantsverdriet, *Appl. Catal. A* **2009**, *354*, 102–110.

[3] M. Saeys, K. F. Tan, J. Chang, A. Borgna, *Ind. Eng. Chem. Res.* **2010**, *49*, 11098–11100; D.-K. Lee, J.-H. Lee, S.-K. Ihm, *Appl. Catal.* **1988**, *36*, 199–207.

[4] X.-Y. Quek, I. A. W. Filot, R. Pestman, R. A. van Santen, V. Petkov, E. J. M. Hensen, *Chem. Commun.* **2014**, *50*, 6005.

[5] R. A. Van Santen, *Acc. Chem. Res.* **2009**, *42*, 57–66.

[6] R. A. van Santen, M. M. Ghouri, S. Shetty, E. J. M. Hensen, *Catal. Sci. Technol.* **2011**, *1*, 891–911.

[7] J. P. den Breejen, P. B. Radstake, G. L. Bezemer, J. H. Bitter, V. Frøseth, A. Holmen, K. P. d. Jong, *J. Am. Chem. Soc.* **2009**, *131*, 7197–7203.

[8] C. Stegelmann, A. Andreasen, C. T. Campbell, *J. Am. Chem. Soc.* **2009**, *131*, 8077–8082; C. T. Campbell, *J. Catal.* **2001**, *204*, 520–524.

[9] P. Biloen, J. N. Helle, W. M. H. Sachtler, *J. Catal.* **1979**, *58*, 95–107; P. Biloen, W. M. H. Sachtler in *Advanced Catal.*, *Vol. 30* (Eds.: H. P. D. D. Eley, B. W. Paul), Academic Press, **1981**, pp. 165–216; R. B. Anderson, *The Fischer–Tropsch Synthesis*, Academic Press, New York, **1984**; Z.-P. Liu, P. Hu, *J. Am. Chem. Soc.* **2002**, *124*, 11568–11569; J. Cheng, X.-Q. Gong, P. Hu, C. M. Lok, P. Ellis, S. French, *J. Catal.* **2008**, *254*, 285–295; X.-Q. Gong, R. Raval, P. Hu, *J. Chem. Phys.* **2005**, *122*, 024711; J. Cheng, P. Hu, P. Ellis, S. French, G. Kelly, C. M. Lok, *Top. Catal.* **2010**, *53*, 326–337.

[10] A. Outi, I. Rautavuoma, H. S. van der Baan, *Appl. Catal.* **1981**, *1*, 247–272; I. C. Yates, C. N. Satterfield, *Energy Fuels* **1991**, *5*, 168–173.

[11] B. W. Wojciechowski, *Catal. Rev.* **1988**, *30*, 629–702.

[12] J. Cheng, P. Hu, *J. Am. Chem. Soc.* **2008**, *130*, 10868–10869.

[13] J. Cheng, P. Hu, P. Ellis, S. French, G. Kelly, M. C. Lok, *J. Phys. Chem. C* **2008**, *112*, 6082–6086.

[14] M. Ojeda, R. Nabar, A. U. Nilekar, A. Ishikawa, M. Mavrikakis, E. Iglesia, *J. Catal.* **2010**, *272*, 287–297; B. T. Loveless, C. Buda, M. Neurock, E. Iglesia, *J. Am. Chem. Soc.* **2013**, *135*, 6107–6121.

[15] A. J. Markvoort, R. A. van Santen, P. A. J. Hilbers, E. J. M. Hensen, *Angew. Chem. Int. Ed.* **2012**, *51*, 9015–9019; *Angew. Chem.* **2012**, *124*, 9149–9153; R. A. Van Santen, A. J. Markvoort, I. A. W. Filot, M. M. Ghouri, E. J. M. Hensen, *Phys. Chem. Chem. Phys.* **2013**, *15*, 17038–17063.

[16] R. A. van Santen, A. J. Markvoort, M. M. Ghouri, P. A. J. Hilbers, E. J. M. Hensen, *J. Phys. Chem. C* **2013**, *117*, 4488–4504.

[17] S. Storsæter, D. Chen, A. Holmen, *Surf. Sci.* **2006**, *600*, 2051–2063; G. Lozano-Blanco, J. Thybaut, W. K. Surla, P. Galtier, G. B. Marin, *Oil Gas Sci. Technol.* **2006**, *61*, 489–496; G. Lozano-Blanco, J. W. Thybaut, K. Surla, P. Galtier, G. B. Marin, *Ind. Eng. Chem. Res.* **2008**, *47*, 5879–5891.

[18] Advance article, "Quantum chemistry of the Fischer–Tropsch reaction catalysed by a stepped Ruthenium surface": I. A. W. Filot, R. A. v. Santen, E. J. M. Hensen, *Catal. Sci. Technol.* **2014**, *4*, 3129–2140.

[19] S. G. Shetty, A. P. J. Jansen, R. A. van Santen, *J. Phys. Chem. C* **2008**, *112*, 14027–14033; S. Shetty, A. P. J. Jansen, R. A. van Santen, *J. Am. Chem. Soc.* **2009**, *131*, 12874–12875.

[20] S. Shetty, R. A. van Santen, *Catal. Today* **2011**, *171*, 168–173.

[21] J. Cheng, P. Hu, P. Ellis, S. French, G. Kelly, C. M. Lok, *J. Phys. Chem. C* **2009**, *113*, 8858–8863.

[22] F. Abild-Pedersen, J. Greeley, F. Studt, J. Rossmeisl, T. R. Munter, P. G. Moses, E. Skúlason, T. Bligaard, J. K. Nørskov, *Phys. Rev. Lett.* **2007**, *99*, 016105.

[23] R. A. v. Santen, M. Neurock, S. G. Shetty, *Chem. Rev.* **2010**, *110*, 2005–2048.

[24] B. Hammer, J. K. Nørskov in *Advanced Catal.*, *Vol. 45* (Ed.: H. K. Bruce C. Gates), Academic Press, New York, **2000**, pp. 71–129; A. Michaelides, Z. P. Liu, C. J. Zhang, A. Alavi, D. A. King, P. Hu, *J. Am. Chem. Soc.* **2003**, *125*, 3704–3705; T. Bligaard, J. K. Nørskov, S. Dahl, J. Matthiesen, C. H. Christensen, J. Sehested, *J. Catal.* **2004**, *224*, 206–217; V. Pallassana, M. Neurock, *J. Catal.* **2000**, *191*, 301–317; J. K. Nørskov, T. Bligaard, A. Logadottir, S. Bahn, L. B. Hansen, M. Bollinger, H. Bengaard, B. Hammer, Z. Sljivancanin, M. Mavrikakis, Y. Xu, S. Dahl, C. J. H. Jacobsen, *J. Catal.* **2002**, *209*, 275–278.

[25] A. C. Lausche, A. J. Medford, T. S. Khan, Y. Xu, T. Bligaard, F. Abild-Pedersen, J. K. Nørskov, F. Studt, *J. Catal.* **2013**, *307*, 275–282.

[26] R. A. van Santen, I. M. Ciobîcă, E. van Steen, M. M. Ghouri in *Advanced Catal.*, *Vol. 54* (Eds.: C. G. Bruce, K. Helmut), Academic Press, New York, **2011**, pp. 127–187.

[27] I. M. Ciobica, F. Frechard, R. A. van Santen, A. W. Kleyn, J. Hafner, *J. Phys. Chem. B* **2000**, *104*, 3364–3369.

[28] I. M. Ciobica, R. A. van Santen, *J. Phys. Chem. B* **2003**, *107*, 3808–3812.

[29] J. Sehested, S. Dahl, J. Jacobsen, J. R. Rostrup-Nielsen, *J. Phys. Chem. B* **2004**, *109*, 2432–2438; M. P. Andersson, F. Abild-Pedersen, I. N. Remediakis, T. Bligaard, G. Jones, J. Engbæk, O. Lytken, S. Horch, J. H. Nielsen, J. Sehested, J. R. Rostrup-Nielsen, J. K. Nørskov, I. Chorkendorff, *J. Catal.* **2008**, *255*, 6–19; J. E. Mueller, A. C. T. van Duin, W. A. Goddard, *J. Phys. Chem. C* **2009**, *113*, 20290–20306.

[30] G. P. Van Der Laan, A. A. C. M. Beenackers, *Catal. Rev.* **1999**, *41*, 255–318; B. Sarup, B. W. Wojciechowski, *Can. J. Chem. Eng.* **1989**, *67*, 620–627.

[31] R. Zennaro, M. Tagliabue, C. H. Bartholomew, *Catal. Today* **2000**, *58*, 309–319.

[32] M. Claeys, E. van Steen in *Stud. Surf. Sci. Catal.*, *Vol. 152* (Eds.: S. André, D. Mark), Elsevier, **2004**, pp. 601–680; E. van Steen, H. Schulz, *Appl. Catal. A* **1999**, *186*, 309–320.

[33] S. G. Shetty, I. M. Ciobica, E. J. M. Hensen, R. A. van Santen, *Chem. Commun.* **2011**, *47*, 9822–9824.